Applicability on Static-Dynamic Verification Method for Seismic Design of Steel Tubular Bridge Piers with Cruciform Plates

Wang Zhanfei[1,*], Sui Weining[2], Toshitaka Yamao[3] and Liang Yongqiang[1]

[1]*Traffic Engineering, Shenyang Jianzhu University, No.9 Hunnan East Road, Hunnan New District, Shenyang, 110-168, China*

[2]*Civil Engineering, Shenyang Jianzhu University, No.9 Hunnan East Road, Hunnan New District, Shenyang, 110-168, China*

[3]*Graduate School of Science and Technology, Kumamoto University, 2-39-1,Kurokami,, Kumamoto, 860-8555,Japan*

Abstract: Steel tubular bridge pier with inner cruciform plates has high seismic performance. In this paper, the applicability of static-dynamic verification method for seismic design of steel tubular bridge piers with inner cruciform plates is studied. The ultimate strength and state of steel tubular stub columns with inner cruciform plate subjected to compression and bending were investigated through finite element analysis. The validity of the proposed design formula of the failure strain which was obtained from the stub column analysis was examined by analysis on tubular steel bridge piers with inner cruciform plates under cyclic loading. The dynamic response analysis of the same steel bridge piers was carried out on the basis of the spring-mass model and the fiber element model. These results indicated the static-dynamic verification method of the seismic response analysis through the spring-mass model are good agreement with dynamic verification method of seismic response analysis by the fiber element model.

Keywords: Steel tubular bridge piers, inner cruciform plates, seismic design, static-dynamic verification, failure stain.

1. INTRODUCTION

Based on the appearance of the severe earthquakes that have occurred in the past decades (e.g. Northridge earthquakes (1994) in USA, Kobe earthquakes (1995) in Japan, Wenchuan earthquakes (2008) in china, Tohoku region earthquakes (2011) in Japan), the research of the seismic performance of bridge structures and the seismic design method of bridge have rapidly developed. In the seismic performance aspect, investigations of the plastic ductility and the limited state of steel bridge piers under cyclic and dynamic loading have been carried out theoretically and experimentally by numbers of research organizations. The aim is to present a new type of steel bridge piers with high ductility during the strong earthquake [1-6]. In recent studies, steel bridge pier with inner cruciform plates have been proposed to improve the seismic performance of steel bridge piers [7-9]. Inner cruciform plates of the steel piers play a similar role as a shear wall in the earthquake-resistant structures. On the other hand, in the seismic design of highway bridges, the performance-based design is newly adopted in many countries [10-16]. This seismic design includes two seismic verification methods under strong ground motions, one of which is the inelastic time-history analysis. That is the verification method of seismic performance-based on dynamic analysis. Although this method is a more powerful procedure for demand predictions, it is time-consuming, which hampers its broader application to common design. In seismic design of complex structures such as arch bridges, cable stayed bridges and suspension bridges, this verification method should be adopted. The other method is non-linear pushover analysis. That is the verification method of seismic performance-based on static analysis. Though there are some assumptions in this analysis, the target structure should be controlled by the fundamental mode. This verification method is widely applied to simple or regular reinforced concrete structures (e.g. Girder Bridge, Frame Bridge) or high-rise building, since both geometric and material non-linearity can be accounted for through the analyses [17-18]. However, non-linear pushover analysis could not be applied to seismic performance verification of steel bridge pier, because steel bridge piers are vulnerable to damage from local and global interaction bucklings under strong ground motion. One of the main efforts made in the study of such structures is to investigate the inelastic behavior of isolated plates or stub-columns. Thus, the static- dynamic verification method for seismic design of the steel bridge is developed [19-21].

*Address correspondence to this author at the Traffic Engineering, Shenyang Jianzhu University, No.9 Hunnan East Road, Hunnan New District, Shenyang, 110-168, China; Tel: +86-24-24694351; Fax: +86-24-24694351;
E-mail: wzf9522@hotmail.com

E-ISSN: 2409-9821/16

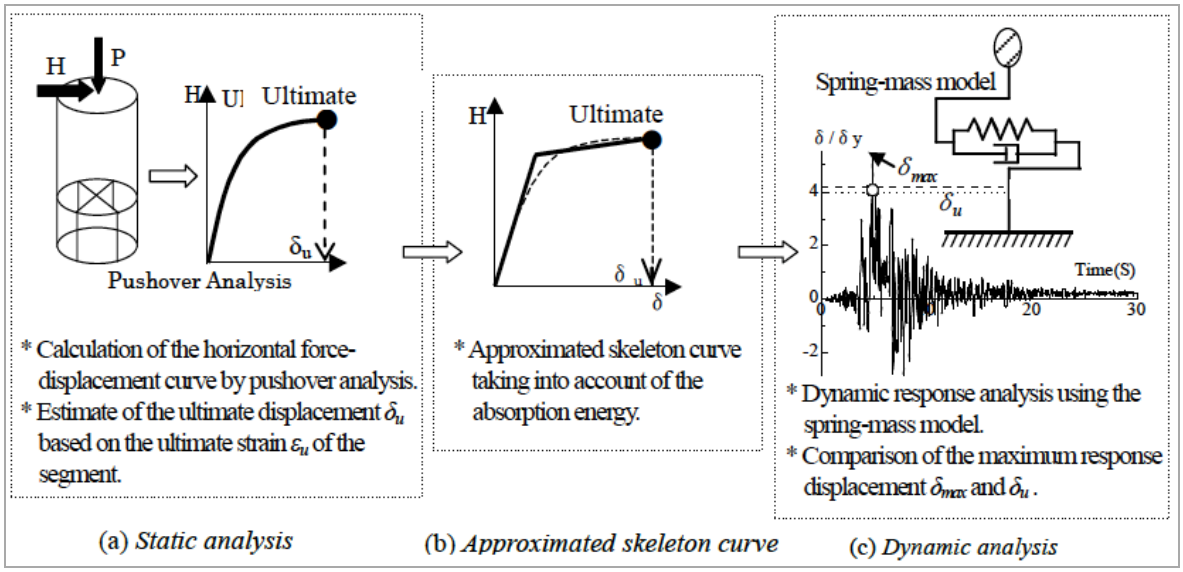

Figure 1: Flow of static-dynamic verification method.

The flow of the static-dynamic verification method is shown in Figure **1**. In order to apply the method to seismic design of the tubular steel bridge pier with inner cruciform plates, it is necessary to clarify the ultimate state (i.e. ultimate displacement and failure strain) of the segment of the steel bridge pier, which is assumed to fail when the steel element reaches the corresponding critical state.

In this paper, the applicability of the static-dynamic verification method for seismic design of steel tubular bridge piers with inner cruciform plates is studied. Firstly, the ultimate strength and the ultimate state of steel tubular stub columns with inner cruciform plate subjected to compression and bending were investigated. The effect of the failure segment length, the radius-to-thickness ratio and the axial load ratio parameter on the ultimate strength and failure strain of the stub columns were examined. Based on the numerical results, design formulas of the ultimate strength and failure strain were proposed for tubular steel bridge piers with inner cruciform plates. Secondly, the validity of the proposed design formula of the failure strain was examined by analysis on tubular steel bridge piers with inner cruciform plates under cyclic loading. Finally, the dynamic response analysis of the same steel bridge piers was carried out through the spring-mass model and the fiber element model. The applicability of the static- dynamic verification method for seismic design of tubular steel bridge piers with inner cruciform plates was demonstrated. In this paper, static analyses were carried out by the finite element package MARC (2005), dynamic analyses were carried out by the non-linear dynamic analytical program TDAPIII (2008).

2. ULTIMATE STATE OF STUB-COLUMN

In the past research, it was found that the local buckling at bottom of a pier has effect on the ultimate strength and ductility of the steel bridge pier with inner cruciform plates. Thus, in order to clarify the failure state of a tubular bridge pier with inner cruciform plates, numerical analysis of stub columns with inner cruciform plates was carried out by the MARC under the combination load of compression and bending. In this analysis, both residual stress and initial deflection have been taken into account.

2.1. Analytical Model of Stub Columns

Analytical model of stub column is shown in Figure **2**. The stub column was divided into 32

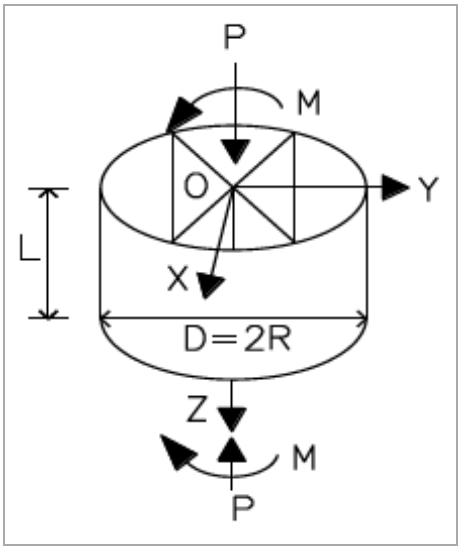

Figure 2: Analytical model of stub column.

elements along the circumference and 5 ~ 20 elements along the longitudinal direction corresponding to the height of the analytical model. Typical finite element meshes of the stub column are shown in Figure **3**. In this analysis, a type of four-node doubly curved thick-shell element (Element 75) provided in the MARC software was adopted. The elasto-plastic and large displacement analysis was carried out with the following main assumptions [22]:

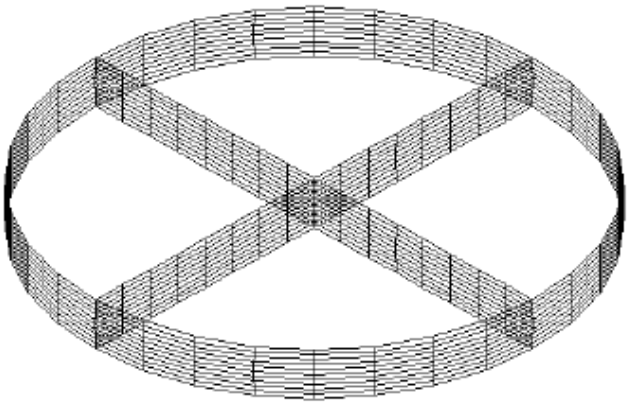

Figure 3: Finite element mesh (32 mesh).

a. Von Mises yield criterion and kinematic hardening rule;

b. Updated-Lagrange procedure;

c. Iterative procedure of full Newton-Raphson method.

The material was assumed to be SS400 steel (JIS) with a yield stress σ_y of 235 Mpa, Young's modulus E of 206 Gpa, and Poisson's ratio ν of 0.3. The stress-strain curve was assumed to be multi-linear as shown in Figure **4**, in which the strain hardening ε_{st} occurs at a strain 10 times of the yield strain ε_y, and the hardening modulus E_{st} is;

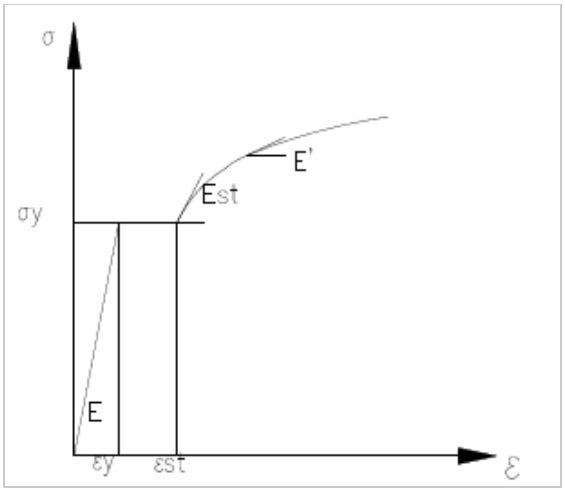

Figure 4: Stress-strain curve of material.

$$\frac{\sigma}{\sigma_y} = 0.556\left\{1-\exp\left[-0.06\left(\frac{\varepsilon}{\varepsilon_y}-10\right)\right]\right\}+1 \quad (\varepsilon_{st}\leq\varepsilon) \qquad (1)$$

An idealized rectangular form of residual stress distribution in inner cruciform plates and the tubular column is adopted due to the welding (Figure **5**) [23].

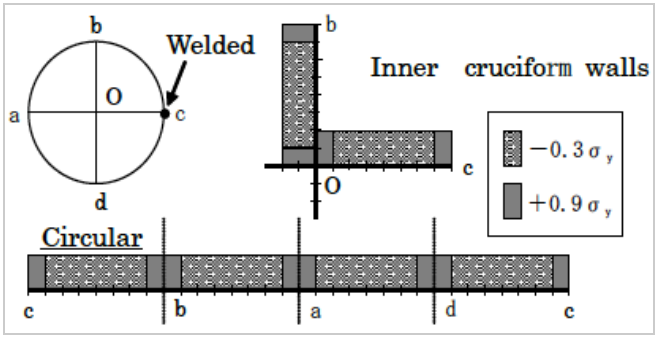

Figure 5: Distribution of residual stress.

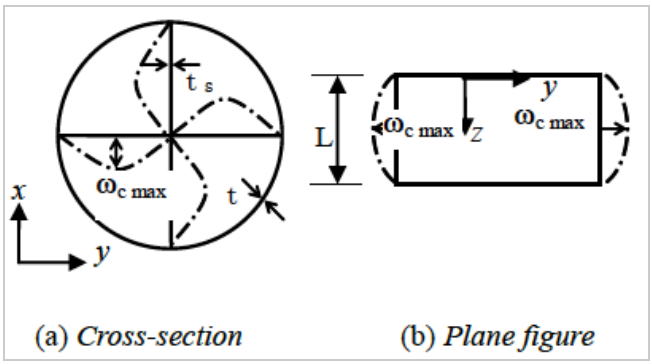

Figure 6: Initial deflection modes.

The initial geometrical deflections also are considered. A sinusoidal initial geometrical deflection curve is applied along the longitudinal directions of the stub E/40. The stress-strain curve was defined by Eq. (1) [23]. The column as shown in Figure **6**(**a**), the initial deflection equation as the following [24]:

$$\omega_c = \omega_{c\max}\sin\left(\frac{\pi z}{L}\right) \qquad (2)$$

In which, ω_c is outward deflection of stub column; ω_{cmax} presents maximum initial displacement (=0.0025L); L is length of the column; R is radius of stub column; z is vertical coordinates in local coordinate system. Moreover, geometrical deflection is considered in cruciform plates, as the following equations [23]:

$$\omega_x = \omega_{c\max}\sin\left(\frac{\pi y}{R}\right)\sin\left(\frac{\pi z}{L}\right) \qquad (3)$$

$$\omega_y = \omega_{c\max} \sin\left(\frac{\pi x}{R}\right) \sin\left(\frac{\pi z}{L}\right) \quad (4)$$

$$\omega_{c\max} = 5.0 \times 10^{-5} \frac{R^2}{t_s} \quad (5)$$

In which, ω_x (or ω_y) is initial deflection of inner plates, R is radius of stub column; t_s is thickness of inner plates; and x and y is longitudinal and circumferential coordinates in local coordinate system, respectively.

Because of the tubular section subjected to compression force or bending moment, a portion between two diaphragms would deform into half sine-waves shape along the column length, which is occurred on local buckling. For this reason, the simply supported at both ends is assumed to simulate as a stub column with a single half-wave of initial deflection by the boundary conditions [25].

2.2. Axial Compressive Analysis

A parametric study of stub columns with inner cruciform plates was firstly carried out under the axial compression. For a given value of a radius-to-thickness ratio, a critical length of the stub column can be obtained expecting the minimum ultimate strength. Then, a relationship between the critical length and the radius-to-thickness ratio was formulated.

The parameters of radius-to-thickness ratio R_t of the stub column and width-to-thickness ratio R_C of inner cruciform plates were defined as the follows.

$$R_t = \frac{R}{t}\frac{\sigma_y}{E}\sqrt{3\left(1-\nu^2\right)} \quad (6)$$

$$R_c = \frac{R}{t_s}\sqrt{\frac{\sigma_y}{E}\frac{12(1-\nu^2)}{4\pi^2}} \quad (7)$$

The effect of L/D (L is a length and D is a diameter of the stub column) was analyzed to establish a design formula for the ultimate strength and the failure strain.

The value of L/D was taken from 0.05 to 0.2 and the six ratios of R_t = 0.05, 0.07, 0.10, 0.15, 0.20 and 0.25. Analytical models with the radius-to-thickness ratio R_c = 0.8 were chosen, because the stub column with this ratio was assumed that the local buckling of the inner cruciform plate would not occur before that of the tubular plate. The numerical results for different values of R_t and L/D shown in Table **1**. Figure **7** shows the plot of the non-dimensionalized ultimate strength σ_u/σ_y versus L/D curves for different values of R_t. For the stub column with the same ratio R_t, and a critical length L_c/D, the minimum ultimate strength was able to obtain. The critical length L_c/D was plotted along the radius-to-thickness ratio R_t corresponding to the critical length L_c in Figure **8**. And the relationship between L_c/D and R_t was determined by the following equation.

$$\frac{L_c}{D} = 0.0415 + \frac{0.0086}{R_t^{0.97}} \quad (8)$$

Table 1: Numerical Results for Parameters of R_t and L/D

R_t	L/D	σ_u/σ_y	R_t	L/D	σ_u/σ_y
0.05	0.050	1.368	0.15	0.060	1.026
	0.100	1.121		0.085	0.977
	0.125	1.065		0.100	0.976
	0.150	1.034		0.110	0.982
	0.175	1.032		0.125	0.995
	0.200	1.031	0.20	0.050	1.013
0.07	0.050	1.282		0.060	0.977
	0.100	1.032		0.075	0.952
	0.125	1.018		0.080	0.950
	0.140	1.017		0.085	0.954
0.10	0.050	1.152		0.100	0.968
	0.100	1.010	0.25	0.050	0.967
	0.120	1.000		0.060	0.939
	0.125	1.007		0.075	0.932
	0.150	1.015		0.085	0.942
	0.175	1.027		0.100	0.969

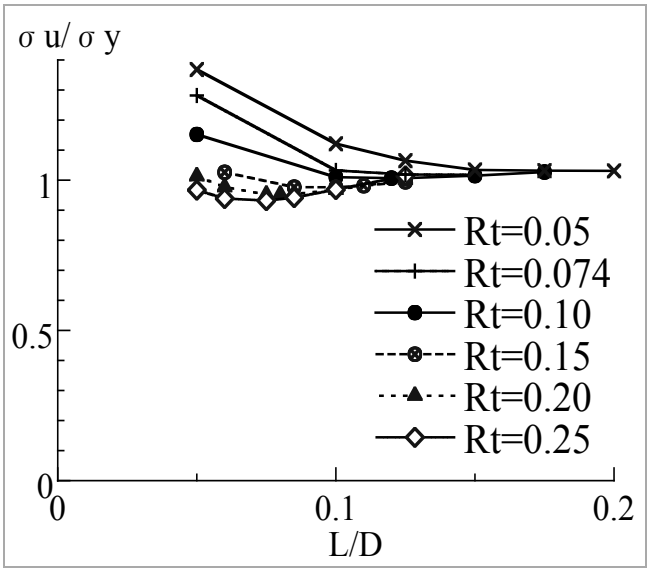

Figure 7: Effect of R_t and L/D on σ_u/σ_y.

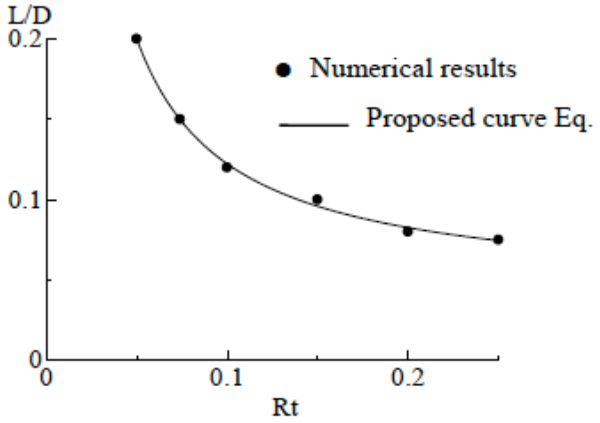

Figure 8: Relationship between L_c/D and R_t and proposed curve.

2.3. Compressive and Bending Analysis

As piers of the bridges are constantly subjected to combined compression and bending, it is needed to investigate the ultimate state of tubular stub columns subjected to compression and bending as shown in Figure **9**.

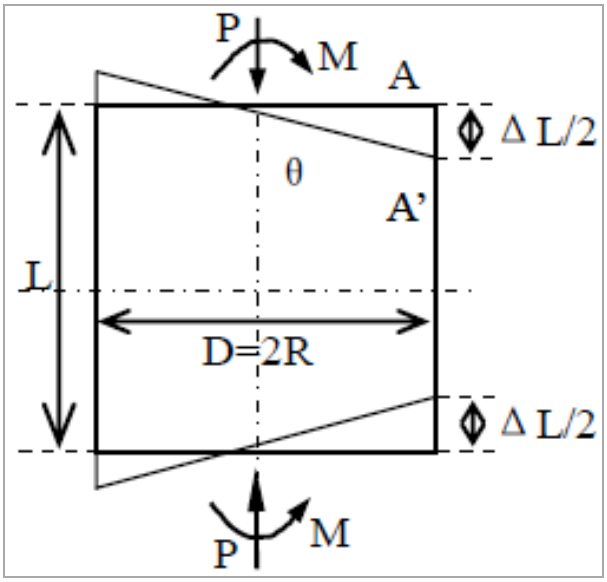

Figure 9: Tubular stub column model subjected to compression and bending.

Table **2** gives the geometrical parameters of the analytical models. Radius-to-thickness ratio R_t of the stub columns with inner cruciform plates ranges from 0.05 to 0.5. Each length of the stub column is determined by Eq. (8). Thickness t is assumed to be 4.5mm for all the tubes, while thickness t_s of the inner cruciform plates varies from 4.5mm to 26.5mm according to R of the tube. To investigate the effect of axial loads on the ultimate strength and strain, the axial load P varies from 0.0 to $0.4P_y$.

Table 2: Geometrical Parameters of Analytical Models

R_t	L/D	t(mm)	t_s(mm)	R (mm)	L (mm)
0.10	0.12	4.5	5.5	239	57.36
0.15	0.10	4.5	8.0	358	71.60
0.20	0.08	4.5	11.0	477	76.32
0.25	0.075	4.5	13.5	597	89.55
0.30	0.069	4.5	15.9	716	98.81
0.40	0.062	4.5	21.0	955	118.42
0.50	0.058	4.5	26.5	1194	138.50

The analysis of stub column model with clamped-simple of the boundary condition was carried out. The initial crookedness and residual stresses were taken to be the same as those in the axial compression case. In the analysis, the moment-strain curve was obtained by applying the rotation angle displacement θ as shown in Figure **9**. Axial strain ε at the outmost compressive edge was computed by the following equations.

$$\varepsilon = \frac{\Delta L}{L} \tag{9}$$

where ΔL is longitudinal displacement of the upper or lower end at the outmost compressive edge

Figure **10** shows the computed failure strain $\varepsilon_u/\varepsilon_y$ (ε_y: yield strain) of the stub columns with inner cruciform plates. The failure strain ε_u is defined as the ultimate strain at the point which is corresponding to 95% of the ultimate strength after the peak load. From this figure, it can be found that values of $\varepsilon_u/\varepsilon_y$ for the same R_t decrease rapidly with the increase of the axial

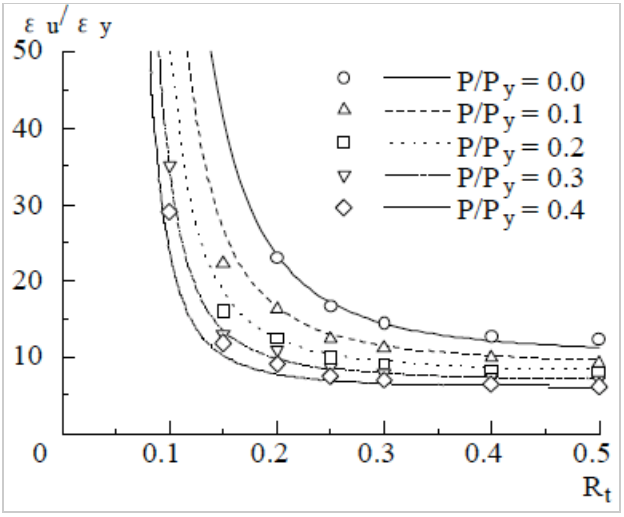

Figure 10: Failure strain of stub column under compression and bending moment.

load, and the values of εu/εy decrease with the increase of R_t for the same axial load.

The numerical results suggest the effects of the axial load and the radius-to-thickness ratio R_t on the behavior of tubular stub columns with inner cruciform plates are significant.

The evaluation of failure strain $\varepsilon_u/\varepsilon_y$ for tubular stub columns is proposed due to the different axial load ratios ranging by the following equations.

$$\frac{\varepsilon_u}{\varepsilon_y}=\frac{0.22\left(1+0.05\frac{P}{P_y}\right)}{(R_t-0.045)^{2.2}\left(1+\frac{P}{P_y}\right)^6}+10\left(1-\frac{P}{P_y}\right) \quad (10)$$

(when $0.1\le R_t\le 0.5$, $0.0\le P/P_y\le 0.4$).

The ultimate bending moment M_u/M_y of all the analytical models is shown in Figure **11**. The ratio of the ultimate bending moment Mu and the yield moment M_y is taken as the vertical axis. As illustrated in Figure **11**, the ultimate bending moment decreases rapidly with the increase of the axial load P/P_y and the radius-to-thickness ratio R_t. A general equation accounting for the effect of both parameters Rt and P/P_y on the ultimate bending moment was found to fit well with the analytical results.

$$\frac{M_{\max}}{M_y}=1.4-1.2\sqrt{R_t-0.045}\left(1-\frac{P}{P_y}\right) \quad (11)$$

$$\left(when, 0.045\le R_t\le 0.50,\quad 0.0\le P/P_y\le 0.4\right)$$

3. CYCLIC ANALYSIS OF STEEL BRIDGE PIERS

To check the validity of the failure strain by Eq.(10), non-linear analysis of tubular steel bridge piers with inner cruciform plates was carried out under the cyclic horizontal load and the constant axial compression load. Not only the geometrical and structural properties of the analytical specimens but also the analytical results are shown on Table **3**. The λ is the slenderness ratio of columns, which is defined by the Eq. (12);

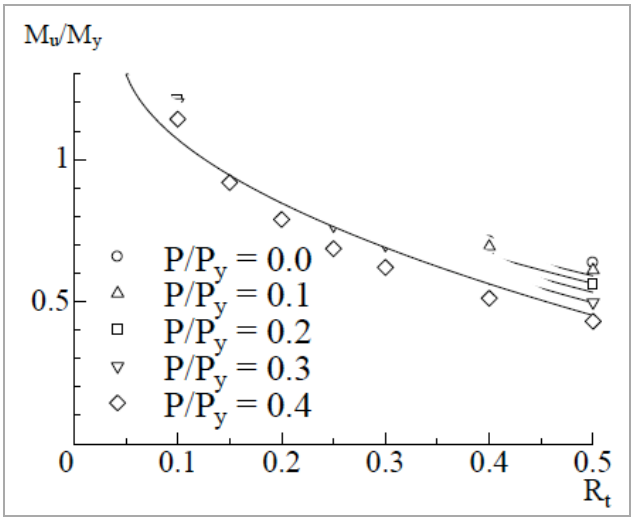

Figure 11: The ultimate bending moment M_u/M_y of all the analytical models.

$$\lambda=\frac{2L_P}{\pi r}\sqrt{\frac{\sigma_y}{E}} \quad (12)$$

In which, r is a radius of gyration of the cross section.

Figure **12** shows the bending moment diagram of the tubular steel bridge pier with inner cruciform plates subjected to the horizontal load and L_0 is the height of the inner cruciform plate. The reasonable height (L_0) of inner cruciform plate is obtained from the condition that the bending moments of bottom segment (as symbol L_c) and hollow segment (as symbol L_e) of the bridge

Table 3: Analytical Specimens of Steel Bridge Pier with Inner Cruciform Walls and Results of Cyclic Loading Analysis (mm)

Specimens	Tube			Inner Walls			λ	R_t	H_y(kN)	δ_y	$H_{0.95}/H_y$	$\delta_{0.95}/\delta_y$	H_s/H_y	δ_s/δ_y
	R	L_P	t	t_S	L_0	L_0/L								
In7430	180	1750	4.5	4.0	577.5	0.33	0.30	0.074	59.5	5.8	1.66	4.05	1.52	4.25
In8315	200	942		6.0	329.5	0.35	0.15	0.083	147.7	1.5	1.67	5.20	1.74	4.00
In8322	200	1442		6.0	504.5	0.35	0.22		96.5	3.6	1.68	4.74	1.66	4.50
In8330	200	1942		6.0	679.5	0.35	0.30		71.6	6.6	1.62	4.20	1.70	4.00
In8338	200	2442		6.0	854.5	0.35	0.38		57.0	10.4	1.63	4.05	1.72	4.00
In9530	230	2250		4.5	787.5	0.40	0.30	0.095	77.7	7.5	1.69	4.10	1.78	4.00
In11630	280	2750		6.4	1237.5	0.45		0.116	101.7	9.2	1.67	4.20	1.72	3.00
In14630	350	3400		7.6	1700.0	0.50		0.146	134.8	11.1	1.65	3.50	1.71	2.50

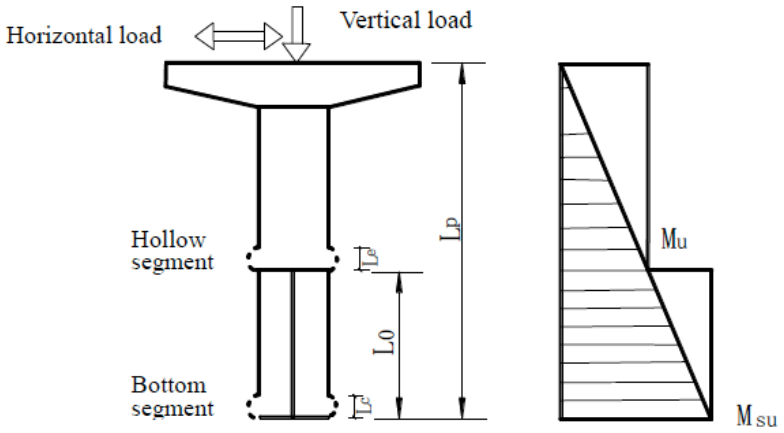

Figure 12: Bending moment diagram of bridge pier.

pier achieve simultaneously the ultimate bending moment. So the height is obtained through the following equation:

$$L_0 = (1 - \frac{M_{su}}{M_u})L_P \quad (13)$$

In which, M_{su} is the ultimate bending moment of steel tubular stub column with hollow section obtained from Ref. 24(1998); Mu is the ultimate bending moment of steel tubular stub column with inner cruciform plates obtained from Eq.(11).

Material properties were the same as those used in previous analysis. In the cyclic analysis, the magnitude of the constant axial load P/P_y was 0.15. At each cycle, the horizontal displacement δ was increased by a value of δ_y (δ_y = yield displacement of bridge pier). (see Yamao *et al*., 2004)

Figure **13** shows the flow of the estimation of the ultimate displacement of the bridge pier with inner cruciform plates under cyclic loading. The strain of the outmost edge of the pier reaches to the ultimate state (symbol ●), when the strain of the outmost edge of the bottom segment is equal to the ultimate strain ε_u obtained by Eq. (10) as shown in Figure **13**(**a**). Then, the ultimate displacement δu is obtained from the applied horizontal displacement corresponding to the ultimate strain εu as shown in Figure **13** (**b**). Figure **14** shows the horizontal load versus horizontal displacement hysteretic and envelope curves for specimens In7430 and In9530. In these analyses, the horizontal load H and the horizontal displacement δ were non-dimensionalized by H_y and δ_y, respectively. Symbols ● and ◎ in Figure **14** represent the ultimate state points. Symbol ● was obtained from the estimation method by Figure **13**(**b**) and symbol ◎ was gotten from the envelope curve corresponding to 95% of the ultimate strength after the peak load. The ultimate displacement obtained by the proposed

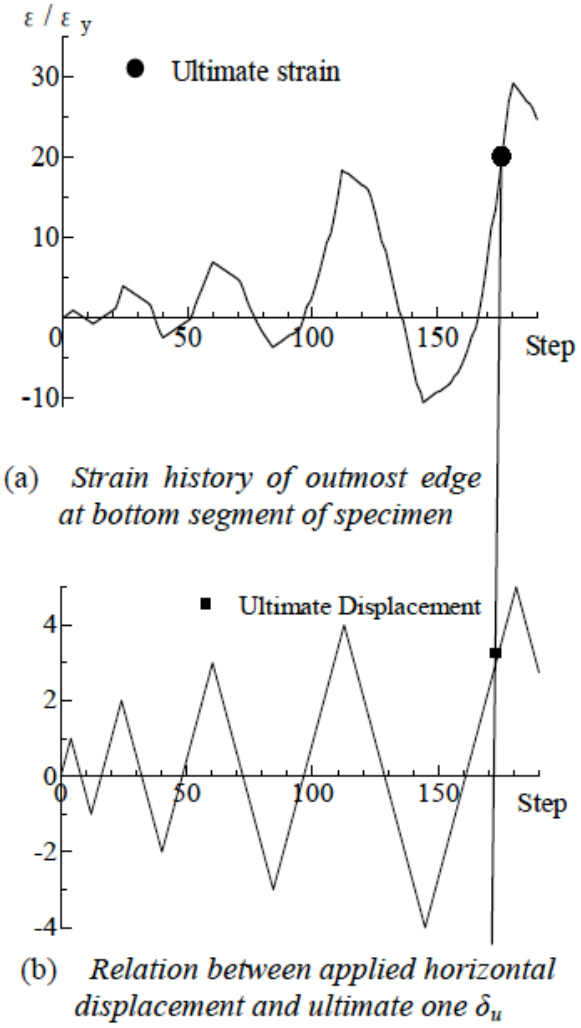

Figure 13: Flow of the estimation of ultimate Displacement δ_u according to failure strain by Eq.(10).

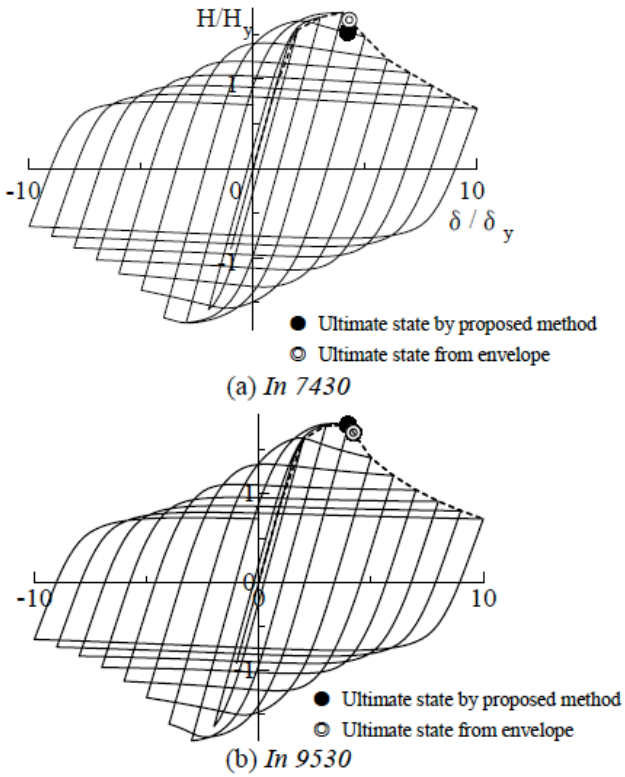

Figure 14: Comparison of the ultimate state obtained from two estimation methods.

method for the pier with inner cruciform plates showed good agreement with the numerical results obtained from the envelope curves. Figure **15** shows the estimated error of ultimate state obtained by the proposed method using the failure strain by Eq.(10) and envelope curves corresponding to 95% of maximum strength after the peak load. From this figure, it is found that the ultimate strength obtained by the proposed method for all specimens shows good agreement with ultimate strength by the envelope curve as shown in Figure **15**(**a**). And the ultimate displacement obtained by the proposed method deviates from ultimate displacement by the envelope curve in some numerical results (see. Figure **15**(**b**)). The main reason is that the ultimate displacement obtained from the applied horizontal displacement corresponding to the failure stain may not take the P-Δ effect for the slender into account.

4. DYNAMIC RESPONSE ANALYSIS

4.1. Analytical Model and Input Seismic Waves

In this section, the dynamic response analysis for the three specimens was carried out using both the spring-mass model and the fiber element model. The spring-mass model in Figure **16**(**b**) composed of a lump mass M, a spring stiffness K and a damping constant C (=0.002), respectively. The approximate skeleton curve for dynamic response analysis was approximated as two straight lines taking the energy absorption into account in horizontal load-displacement curve obtained by the pushover analysis as shown in Figure **16**(**a**). The initial gradient of this curve was assumed to have the stiffness K_0, and the second gradient the stiffness K_1. Table **4** represents the structural parameters of the skeleton curve and the spring-mass model.

In order to investigate the validity of the dynamic analysis by the spring-mass model, the numerical

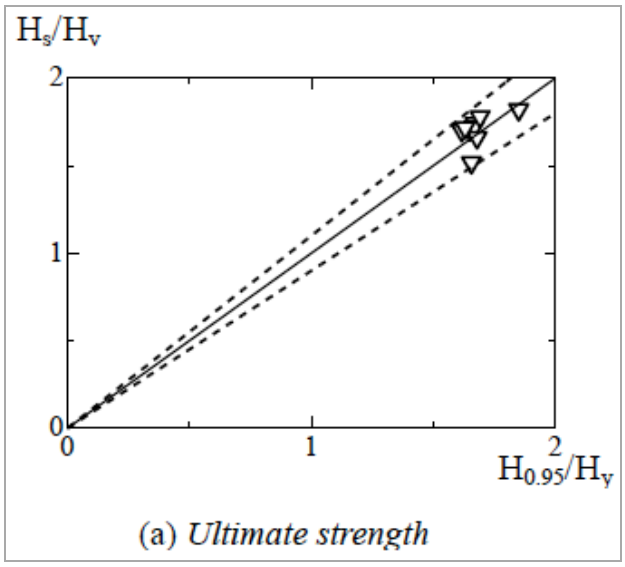

Figure 15: Estimated error of ultimate state obtained by proposed method and envelope curve corresponding to 95% of maximum strength after the peak load.

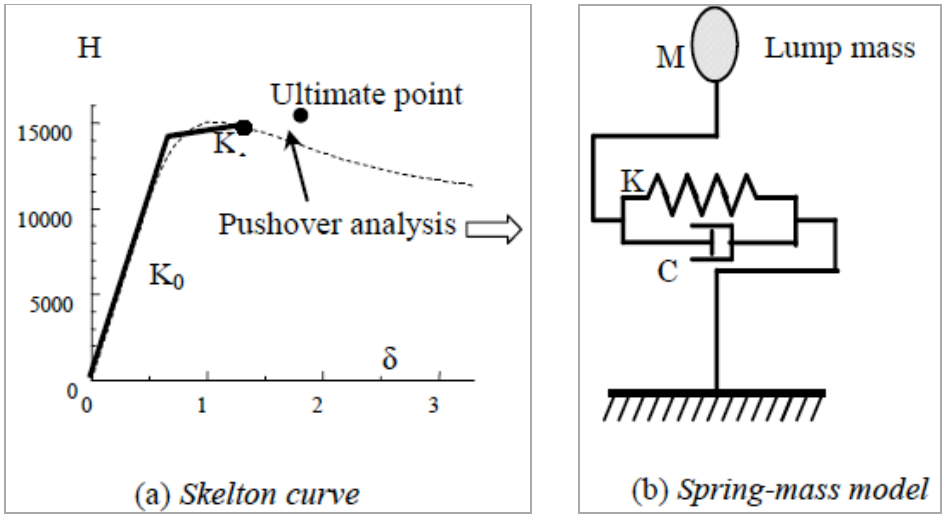

Figure 16: Approximated skeleton curve and spring-mass model.

results were compared with the dynamic analysis using the fiber beam element model. The fiber model was modeled by 34 fiber-beam elements as shown in Figure **17**.

Table 4: Structural Parameters of Skeleton Curve and Spring-Mass Model

Model names	K_0 (kN/mm)	K_1/K_0	δ_y (mm)	M (kg)
In8330	9.49	0.012	11.1	20100
In9530	9.67	0.003	13.5	23200
In7430	10.91	0.007	20.1	35400

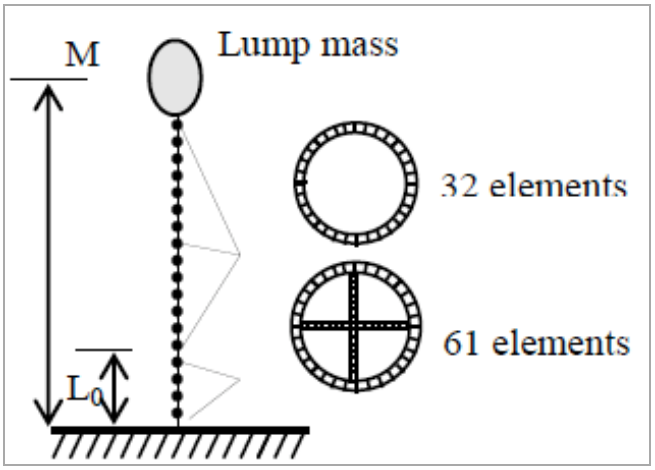

Figure 17: Fiber element model.

Two input seismic waves used in the dynamic response analysis are shown in Figure **18**. These waves were recorded by the Japan Meteorological Agency (JMA) and the Japanese Railway Takatori Station (JRT) as strong ground motion. Numerical analysis was conducted by the nonlinear dynamic program TDAPⅢ(2008). A constant time step of 0.001sec was utilized. The seismic response analysis with 1.2 times acceleration waves of JMA and JRT were used to reach ultimate state of the column with inner cruciform plates.

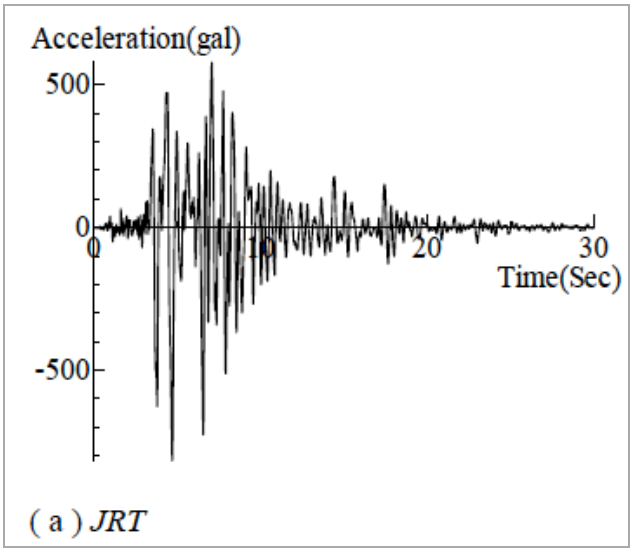

Figure 18: Input seismic waves.

4.2. Numerical Results

Figure **19** shows the H-δ hysteretic curves at the top of the model subjected to JMA and JRT waves. The vertical axis y is the ratio of the horizontal reaction H at the bottom of the column and the yield horizontal load H_y. The horizontal axis x is the ratio of the horizontal displacement δ at the top of the column and the yield displacement δ_y. In these figures, solid lines represent numerical results through the dynamic analysis using the spring-mass model, and dashed lines indicate

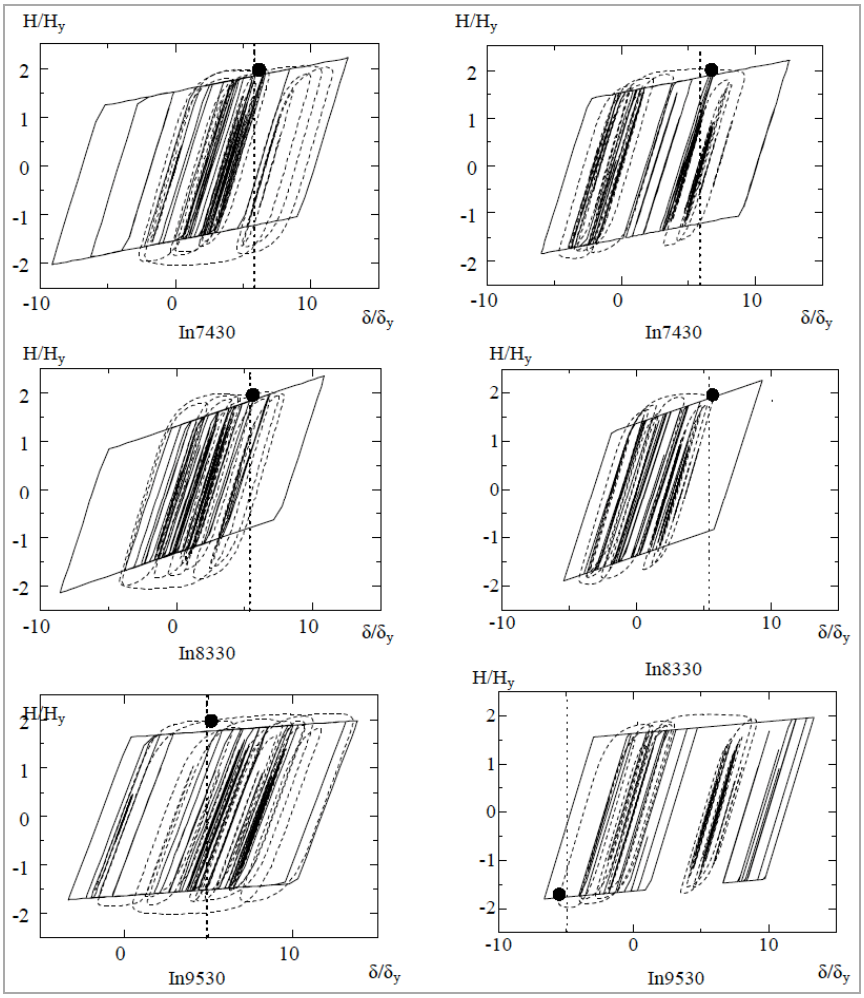

Figure 19: Comparison of the H- δ hysteretic curves using spring-mass model and fiber beam model, and of the estimated ultimate displacement.

numerical ones through the dynamic analysis using the fiber beam element model. Vertical dotted lines represent the ultimate displacement δ_u obtained by proposed method. Symbol ● was ultimate displacement obtained by the fiber beam model. It can be found that the ultimate displacement δ_u by the proposed method shows good agreement with the ultimate displacement point by the fiber beam model. Though, the responsive displacement of spring-mass model is larger than that of fiber beam model. From the results, the validity of static-dynamic verification method for tubular columns with inner cruciform plates is demonstrated.

CONCLUSIONS

In this study, applicability of static-dynamic verification method for seismic design of steel tubular bridge piers with inner cruciform plates was investigated. Numerical analysis was carried out by analytical programs MARC and TDAPⅢ. The main conclusions obtained by this study are summarized as follows.

1) The failure strain and ultimate strength of tubular bridge piers with inner cruciform plates are obtained by the FEM analysis of tubular stub columns.

2) The ultimate state by the proposed method for the column shows good agreement with numerical results obtained from the envelope curve beside of slenderness column with inner cruciform plates.

3) The ultimate displacement δ_u obtained by the proposed method based on failure strain ε_u through Eq. (10) shows good agreement with the ultimate displacement point by the dynamic analysis using the fiber element model.

4) From the numerical results, the validity of static-dynamic verification method for tubular columns with inner cruciform plates is demonstrated.

REFERENCES

[1] Usami T, Lu ZH, Ge HB and Kono T. Seismic performance evaluation of steel arch bridges against major earthquakes. Part 1 Dynamic analyses approach. Earthquake Engineering and Structural Dynamics 2004; 3: 1337-1354. http://dx.doi.org/10.1002/eqe.407

[2] Kono T, Ge HB and Usami T. Re-examination of the ultimate strain formula for steel box stub-columns and its application in steel arch bridges. Proceedings of the 6th Symposium on Ductility Design Method for Bridges, Ductility Design Subcommittee, Earthquake Engineering Committee, JSCE, Tokyo, Japan 2003; 323-328.

[3] Iura M, Orino A and Ishizawa T. Elasto-Plastic Behavior of Concrete-Filled Steel Tubular Columns. Journal of Structural Mechanics and Earthquake Engineering, JSCE 2002; No. 696/I-58: 285-298.

[4] Kazuo Chu and Takamasa Sakurai. A Study for Seismic Reinforcement Method on Existing Cylindrical Steel Piers by Weld Rectangular Steel Plates. Journal of structure engineering 2003; 49A: 139-144.

[5] Julia M and Michel B. Cyclic testing of concrete-filled circular steel bridge piers having encased fixed-based detail [J]. Journal of Bridge Engineering ASCE 2004; 9(1): 14-23. http://dx.doi.org/10.1061/(ASCE)1084-0702(2004)9:1(14)

[6] Michel B and Julia M. Seismic design of concrete-filled circular steel bridge piers [J]. Journal of Bridge Engineering, ASCE 2004; 9(1): 24-34. http://dx.doi.org/10.1061/(ASCE)1084-0702(2004)9:1(24)

[7] Yamao T, Iwatsubo K, Itoh M and Matsumura S. Experimental Study on Ductility and Seismic Behavior of Steel Tubular Bridge Piers under Cyclic Loading. Proceedings of the Sixth Pacific Structural Steel Conference, China 2001; 502-507.

[8] Yamao T, Iwatsubo K, Yamamuro T, Ogushi M and Matsumura S. Steel bridge piers with inner cruciform plates under cyclic loading. Thin-Plateed Structures 2002; 40(2): 183-197. http://dx.doi.org/10.1016/S0263-8231(01)00059-3

[9] Wang zhanfei and Yamao T. Ultimate strength and Ductility of Stiffened Steel Tubular Bridge Piers. International Journal of steel structures 2001; 11(1): 81-90.

[10] Japan Road Association. Design Specifications for Highway Bridges, Part V. Seismic Design. Maruzen Co., Ltd, Japan. (in Japanese) 2002.

[11] Japan Road Association. Design Specifications for Highway Bridges, Part II Steel Bridge. Maruzen Co., Ltd, Japan. (in Japanese) 2002.

[12] Japan Road Association. Design Specifications for Highway Bridges, Part V Seismic Design. Maruzen Co., Ltd, Japan. (in Japanese) 2012.

[13] People Republic of China Ministry of Housing and Urban-Rural Development: Code for seismic design of urban bridge (CJJ 166-2011), [M]. Beijing: China Architecture and Building Press. (in Chinese) 2011.

[14] People Republic of China Ministry of Transport. Guidelines for seismic Design of Highway Bridge [M]. Beijing: Communications Press. (in Chinese) 2008.

[15] Caltrans. Bridge Memo to Designers-seismic design Methodology [M], California Department of Transportation, Sacramento 1999.

[16] Caltrans. Seismic Design Criteria [M], Vers.1.0, California Department of Transportation, Sacramento 1999.

[17] John L Bignell, James M LaFave and Neil M Hawkins. Seismic vulnerability assessment of plate pier supported highway bridges using nonlinear pushover analyses. Engineering Structures 27: 2044-2063.

[18] Chopra AK, Goel RK and Chintanapakdee C. Statistics of single-degree-of-freedom estimate of displacement for pushover analyses of buildings. Journal of Structural Engineering (ASCE) 2003; 129: 459-469. http://dx.doi.org/10.1061/(ASCE)0733-9445(2003)129:4(459)

[19] Usami T, Yi Zheng and Hanbin Ge. Seismic Design Method for Thin-Plateed Steel Frame Structures. Journal of Structural Engineering 2001; 127(2): 137-144. http://dx.doi.org/10.1061/(ASCE)0733-9445(2001)127:2(137)

[20] Yi Zheng, Tsutomu Usami and Hanbin Ge. Seismic response predictions of multi-span steel bridges through pushover analysis. Earthquake Engineering and Structural Dynamics 2003; 32: 1259-1274. http://dx.doi.org/10.1002/eqe.272

[21] Zhihao Lu, Tsutomu Usami and Hanbin Ge. Seismic performance evaluation of steel arch bridges against major earthquakes. Part 2: Simplified verification procedure, Earthquake Engineering and Structural Dynamics 2004; 33: 1355-1372. http://dx.doi.org/10.1002/eqe.406

[22] MSC. Software Corporation, User manual Volume A-E. MSC Japan Ltd.. Japan. (in Japanese) 2005.

[23] Usami T. Guidelines for Stability Design of Steel Structures 2nd Edition [M], Japan Society of Civil Engineering, Tokyo (in Japanese) 2005.

[24] Shengbin Gao, Tsutomu Usami and Hanbin Ge. Ductility Of Steel Short Cylinders In Compression And Bending. Journal of Engineering Mechanics 1998; 124(2): 176-183. http://dx.doi.org/10.1061/(ASCE)0733-9399(1998)124:2(176)

[25] Lilya Susanti, Akira Kasai and Yuki Miyamoto. Postbuckling behavior of welded box section steel compression members. International Journal of Civil Engineering and Technology (IJCIET) 2015; 6: 65-78.

Received on 25-03-2016 Accepted on 26-05-2016 Published on 14-10-2016

DOI: http://dx.doi.org/10.15377/2409-9821.2016.03.01.1